Research paper

Novel spherical-planar and Bennett-spherical 6R metamorphic linkages with reconfigurable motion branches

Xuesi Ma [a], Ketao Zhang [b], Jian S Dai [c],*

[a] MoE Key Laboratory for Mechanism Theory and Equipment Design, International Centre for Advanced Mechanisms and Robotics, School of Mechanical Engineering, Tianjin University, Tianjin 300072, PR China
[b] The Center for Advanced Robotics, Queen Mary University London, London E1 4NS, UK
[c] Advanced Kinematics and Reconfigurable Robotics Lab, Center for Robotics Research, King's College London, Strand, London WC2R 2LS, UK

ARTICLE INFO

ABSTRACT

A metamorphic linkage is capable of changing its motion branches and can be used as mechanisms for reconfigurable robots for various tasks. This paper presents two novel metamorphic linkages as the spherical-planar 6R metamorphic linkage and the Bennett-spherical 6R metamorphic linkage both of which have three various distinguished motion branches. Having established the close-loop equation of the spherical-planar 6R metamorphic linkage, the paper reveals the conditions of various motion branches and a set of transformations for switching motion branches. The paper further uses to reveal the inherent properties of this over-constrained metamorphic 6R linkage that is able to perform both spherical and planar motion with mobility one. Because of geometrical constraints at bifurcation points, the linkage is able to reconfigure to the deployed spherical motion branch, the planar motion branch and the folded spherical motion branch. The two spherical motion branches could be seen on both a large sphere that presents the deployed spherical motion and a small sphere that presents the folded spherical motion. This leads to the revelation of the novel Bennett-spherical 6R metamorphic linkage that has the transition from one deployed Bennett configuration branch to a spherical configuration branch and then to another folded Bennett configuration branch. Given the geometric parameters of both metamorphic linkages, it reveals that these linkages are special cases of Bricard line-symmetric 6R linkage.

© 2018 Published by Elsevier Ltd.

1. Introduction

Over-constrained linkages are a kind of special linkages that mobility does not satisfy the Grübler–Kutzbach [1] formula. 6R close-loop linkages with mobility one are typical over-constrained linkages. The world first over-constrained 6R linkage was Sarrus linkage [2]. Bricard [3,4] investigated a group of 6R linkages that can be classified into line-symmetric octahedral, plane-symmetric octahedral, doubly collapsible octahedral cases and general line-symmetric, plane-symmetric and trihedral 6R linkages and proved mobility of the first three linkages is one with all axes in a linear complex. Myard [5] presented a 6R linkage by combining two complementary Bennett linkages [6]. Schatz [7] presented an over-constrained linkage that was widely used in industrial mixing machines. Goldberg [8] gave a group of 6R linkages that are classified into series,

* Corresponding author at: Center for Robotics Research, King's College London, University of London, Strand, London WC2R 2LS, UK.
  E-mail address: jian.dai@kcl.ac.uk (J.S. Dai).

L-shaped, generalized 6R linkages. Altman [9] identified a 6R linkage which is a special case of Bricard linkage. Waldron [10] investigated a hybrid 6R linkage as the combination of two Bennett linkages on a common joint by constraining the relative position of joints. Baker [11] analyzed all kinds of Bricard linkages and provided the close loop equations for all these linkages. Wohlhart presented a 6R linkage [12] that exists a line intersecting all joint axes by combining two Goldberg 5R linkages as the double-Goldberg linkage. Chen and You [13] presented a 6R linkage in the same way. Cui and Dai [14] put forward a double-center 6R linkage and gave the axis constraints for this kind of linkages. Zhang and Dai [15] analyzed an over-constrained 6R linkage with 2-fold rotational symmetry and they regarded it as a case of Bricard linkage. Kong [16] presented a method to design over-constrained 6R linkages using symmetric planar 4R linkage and spherical 4R linkage. All these linkages are classical over-constrained 6R linkages and have only one motion branch. Though the 6R linkage with 2-fold rotational symmetry [15] has two motion branches, but no method is given for designing the linkage with more than one motion branch.

Reconfigurable linkages were revealed in 1990s. There were two kinds of reconfigurable linkages then as kinematatropic linkages presented by Wohlhart [17] and metamorphic linkages proposed by Dai and Rees Jones [18]. They are reconfigurable when they run to bifurcation or multifurcation points. In metamorphic linkages, it was found that some linkages can change their topologies as origami arts act where the transformation of metamorphic linkages can be described by a matrix method [19]. In this century, Galletti and Fanghella [20] presented four single loop kinematatropic linkages and put forward a synthesis method for this kind of linkages. Yan and Liu [21] presented linkages with variable topologies as a type of reconfigurable linkages. Lee and Hervé [22] proposed a type of linkages with discontinuous degree of freedom. In the past ten years, with the development of reconfigurable rT joint [23] and vA joint [24], metamorphic parallel mechanisms were proposed and some single loop reconfigurable linkages [25,26] were proposed. Ye et al. [27] used the discontinuous degree of freedom linkage as a compound joint to investigate a reconfigurable parallel mechanism. Zhang and Dai [28] presented a metamorphic linkage with a trifurcation point by making one limb as Sarrus linkage concurrent. Qin et al. [29] extended the bifurcation points to multi-furcation points and therefore extended the concept of reconfigurable linkages. Synthesis for metamorphic linkages was proposed in [30,31].

It is found that constraint singularity often provides furcation points. As indicated by Hunt [32] Sugimoto et al. [33], some special points where the linkages were not determinate, that implicitly indicating that motion could be changed at these points. Zlatanov et al [34] therefore put the linkages into a configuration space that is divided into distinct regions by constraint singularity points. Müller [35] put forward that the higher derivatives of the configuration of a rigid body system that reflects motion-change characteristics of a linkage.

The reconfigurable parallel mechanisms [23,24,27] and the reconfigurable single loop linkages [25,26,28,29] are the practical cases of reconfigurable mechanisms and they are analyzed using screw theory. The method [30,33–35] for analyzing the singularity and bifurcation of mechanisms are all based on screw theory [36]. This leads us to use screw theory to design and analyze reconfigurable over-constrained 6R linkages.

With all above development, reconfiguration of 6R over-constrained linkages has not yet been thoroughly revealed and the potential nature of reconfiguration in these linkages has not been identified with new 6R over-constrained linkages still to be revealed. This paper presents two novel metamorphic 6R linkages, the spherical-planar metamorphic linkage and the Bennett-spherical metamorphic 6R linkage. The former is extracted from a kirigami fold while the latter is reveled from the study of the transition index. The paper analyzes these 6R metamorphic linkages and provides the transition index to describe the reconfiguration between motion branches. Section 2 deals with the spherical-planar metamorphic linkage from a kirigami and its close-loop equation. Three motion branches in both deployed and folded spherical motion branches and in planar motion branch are found and their corresponding geometrical constraints are given. Section 3 to Section 5 deal with the motion and reconfiguration of the three motion branches. From spherical motion branches to planar motion branch, motion and reconfiguration are analyzed. The transformation of the linkage and the close path of a point are given. The transition index is used to describe the reconfiguration of the linkage and to design a new 6R metamorphic linkage. This leads to the novel Bennett-spherical 6R metamorphic linkage, with its deployed and folded Bennett configuration branches and with its spherical motion branch in Section 6. The three motion branches and the close-loop transformation are given in this section.

2. Spherical-planar 6R metamorphic linkage and its close loop equation

Taking creases as revolute joints and rigid panels as links based on the principle set up in [18], the folded Kirigami in Fig. 1 equates to a closed-loop mechanism, which is termed spherical-planar metamorphic 6R linkage here.

2.1. From a kirigami fold to the spherical-planar metamorphic linkage

As shown in Fig. 1(a), the kirigami fold is cut out of a piece of paper in square shape with side length l. O is the center of the square and φ_1 is the angle between OA' and the side. The two lines OA and OA' are symmetric with respect to OO_1, thus $|OA|$ equals to $|OA'|$. The points O_1, O_1' and O_1'' are on a circle with center O and radius a, meaning $|OO_1|$, $|OO_1'|$ and $|OO_1''|$ equal to a, respectively. The creases OB and O_1C are parallel and perpendicular to O_1O_1' while the creases OD and $O_1''E$ are parallel and perpendicular to O_1O_1''. The geometry of the kirigami is defined by a and φ_1. Attaching $O_1'A$ and $O_1''A'$, we obtain a closed-loop kirigami in Fig. 1(b).
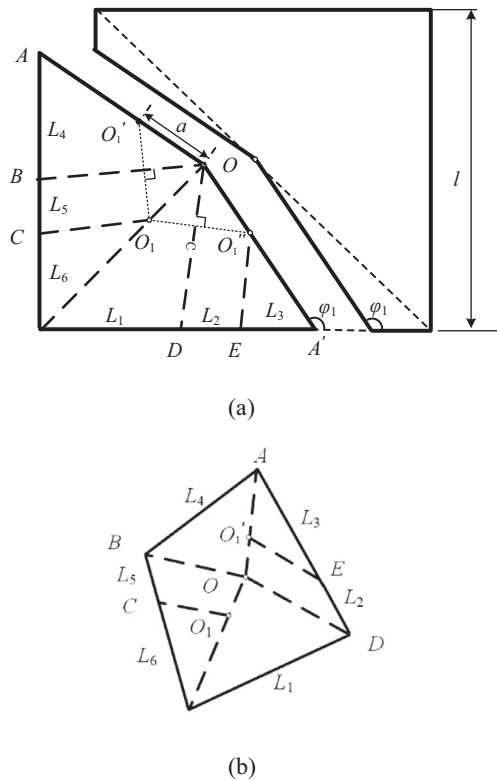
(a)

(b)

Fig. 1. The kirigami fold and its dimensions. (a). The open-loop kirigami. (b) The close-loop kirigami.

Taking the panels as links and creases as revolute joints, a linkage is extracted as shown in Fig. 2. Since creases $O_1'A$ and $O_1''A'$ are aligned to each other in the closed-loop form of the kirigami in which O_1' is coincide with O_1'', the axis of revolute joint $\boldsymbol{S}_4$ of the extracted linkage represents the jointed axes of $\boldsymbol{S}_4'$ and $\boldsymbol{S}''_4$.

According to the parameters of the kirigami in Fig. 1, the D-H parameters of the linkage in Fig. 2(a) are given by

$$a_{23} = a_{56} = a \cos\left(\frac{\varphi_1}{2} - \frac{\pi}{8}\right), a_{12} = a_{34} = a_{45} = a_{61} = 0$$

$$\alpha_{12} = \alpha_{34} = \alpha_{45} = \alpha_{61} = \frac{\varphi_1}{2} - \frac{\pi}{8}, \alpha_{23} = \alpha_{56} = 0$$

$$d_1 = d_4 = a, d_2 = d_5 = 0, d_3 = d_6 = -a\sin\left(\frac{\varphi_1}{2} - \frac{\pi}{8}\right) \tag{1}$$

2.2. Close loop equation of the spherical-planar metamorphic linkage

The kinematic model of the linkage is shown in Fig. 3. The fixed coordinate frame is set with origin O located at the intersection of joints $\boldsymbol{S}_1$ and $\boldsymbol{S}_2$, z axis aligned to axis of joint $\boldsymbol{S}_1$, x axis normal to both $\boldsymbol{S}_1$ and $\boldsymbol{S}_2$ and y axis following the right-hand rule. The moving coordinate frame is attached to link L_4 with the origin O_m located at the intersection of joints $\boldsymbol{S}_4$ and $\boldsymbol{S}_5$, z_m axis aligned to axis of joint $\boldsymbol{S}_4$, x_m axis normal to both joint $\boldsymbol{S}_4$ and joint $\boldsymbol{S}_5$ and y_m axis decided by right-hand rule.

In the limb with joints $\boldsymbol{S}_2$, $\boldsymbol{S}_3$ and $\boldsymbol{S}_4$ in Fig. 3(a), the transformation matrix of moving coordinate frame is given by

$$\boldsymbol{T}_1 = \boldsymbol{T}_{12}\boldsymbol{T}_{23}\boldsymbol{T}_{34} \tag{2}$$

where

$$\boldsymbol{T}_{ij} = \begin{bmatrix} 1 & 0 & 0 & a_{ij} \\ 0 & \cos\alpha_{ij} & -\sin\alpha_{ij} & 0 \\ 0 & \sin\alpha_{ij} & \cos\alpha_{ij} & 0 \\ 0 & 0 & 0 & 1 \end{bmatrix} \begin{bmatrix} \cos\theta_j & -\sin\theta_j & 0 & 0 \\ \sin\theta_j & \cos\theta_j & 0 & 0 \\ 0 & 0 & 1 & d_j \\ 0 & 0 & 0 & 1 \end{bmatrix} \tag{3}$$

in which α_{ij}, a_{ij}, d_j are the D-H parameters in Eq. (1), θ_j is the angle of joint j.
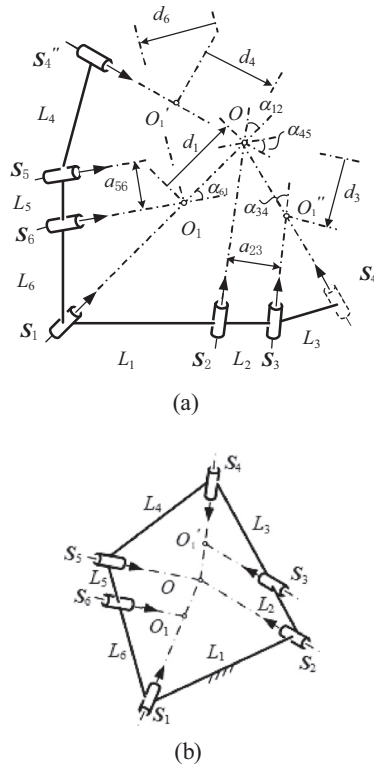
(a)

(b)

Fig. 2. The spherical-planar metamorphic linkage from kirigami and its parameters. (a)The parameters of the extracted kinematic chain. (b). The spherical-planar linkage corresponding to the closed-loop kirigami.

From the limb of S_1, S_6 and S_5 in Fig. 3(b), the homogeneous transformation is given by

$$T_2 = T_{16}T_{65}T_{54} \tag{4}$$

where

$$
T_{kl} = \begin{bmatrix} \cos\theta_k & \sin\theta_k & 0 & 0 \\ -\sin\theta_k & \cos\theta_k & 0 & 0 \\ 0 & 0 & 1 & -d_k \\ 0 & 0 & 0 & 1 \end{bmatrix} \begin{bmatrix} 1 & 0 & 0 & -a_{lk} \\ 0 & \cos\alpha_{lk} & \sin\alpha_{lk} & 0 \\ 0 & -\sin\alpha_{lk} & \cos\alpha_{lk} & 0 \\ 0 & 0 & 0 & 1 \end{bmatrix} \tag{5}
$$

in whichα_{lk}, a_{lk}, $d_k$are the D-H parameters in Eq. (1), θ_k is the angle of joint i.

Because two transformation matrices describe the same moving coordinate frame O_m-$x_m y_m z_m$, T_1 and T_2 are equal and a closed-loop equation can be obtained as

$$T_{12}T_{23}T_{34} = T_{16}T_{65}T_{54} \tag{6}$$

For a physical model, we choose $a = \frac{\sqrt{2}l}{5}$ and $\varphi_1 = \frac{3}{4}\pi$. Thus, all the parameters of the linkage are given. Substituting them into Eq. (6), we can obtain the homogenous transformation matrix. The translational part of the matrix on the left side is

$$
\mathbf{r}_{O_m} = \begin{pmatrix} \frac{l}{5}(\cos\theta_2 + \sin(\theta_2 + \theta_3)) \\ \frac{\sqrt{2}l}{10}(\sin\theta_2 - \cos(\theta_2 + \theta_3)) \\ \frac{\sqrt{2}l}{10}(\sin\theta_2 - \cos(\theta_2 + \theta_3)) \end{pmatrix} \tag{7}
$$

The matrix on the right side is derived as

$$
\mathbf{r}_{O_m} = \begin{pmatrix} \frac{l}{5}\left(-\cos\theta_6\cos\theta_1 + \frac{\sqrt{2}}{2}\sin\theta_6\sin\theta_1 + \frac{\sqrt{2}}{2}\sin\theta_1\right) \\ \frac{l}{5}\left(\cos\theta_6\sin\theta_1 + \frac{\sqrt{2}}{2}\sin\theta_6\cos\theta_1 + \frac{\sqrt{2}}{2}\cos\theta_1\right) \\ \frac{l}{5}\left(-\frac{\sqrt{2}}{2} - \frac{\sqrt{2}}{2}\sin\theta_6\right) \end{pmatrix} \tag{8}
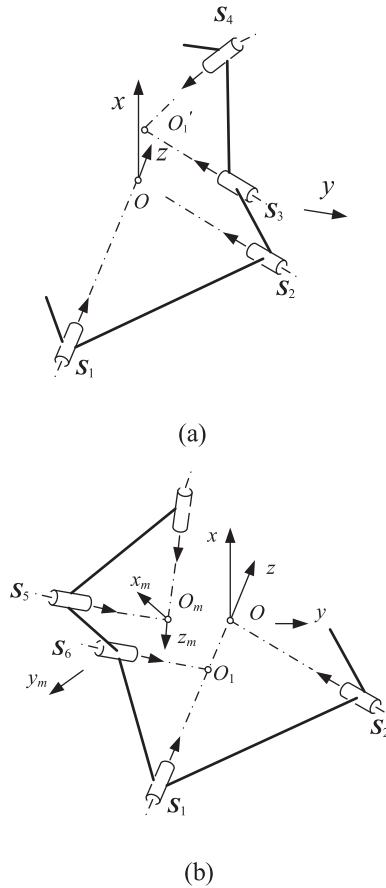$$

(a)

(b)

Fig. 3. Geometric model of two limbs. (a). Limb of joints 2, 3 and 4. (b). Limb of joints 1, 6 and 5.

According to Eqs. (7) and (8), we have

$$\frac{l}{5}(\cos\theta_2 + \sin(\theta_2 + \theta_3)) = \frac{l}{5}\left(-\cos\theta_6\cos\theta_1 + \frac{\sqrt{2}}{2}\sin\theta_6\sin\theta_1 + \frac{\sqrt{2}}{2}\sin\theta_1\right) \tag{9}$$

$$\frac{\sqrt{2}l}{10}(\sin\theta_2 - \cos(\theta_2 + \theta_3)) = \frac{l}{5}\left(\cos\theta_6\sin\theta_1 + \frac{\sqrt{2}}{2}\sin\theta_6\cos\theta_1 + \frac{\sqrt{2}}{2}\cos\theta_1\right) \tag{10}$$

$$\frac{\sqrt{2}l}{10}(\sin\theta_2 - \cos(\theta_2 + \theta_3)) = \frac{l}{5}\left(-\frac{\sqrt{2}}{2} - \frac{\sqrt{2}}{2}\sin\theta_6\right) \tag{11}$$

The D-H parameters in Eq. (1) and the closed-loop equation reveals that the linkage in Fig. 2(b) is a special case of Bricard line-symmetric 6R linkage. According to Baker [37], the joint angles satisfy the following equation
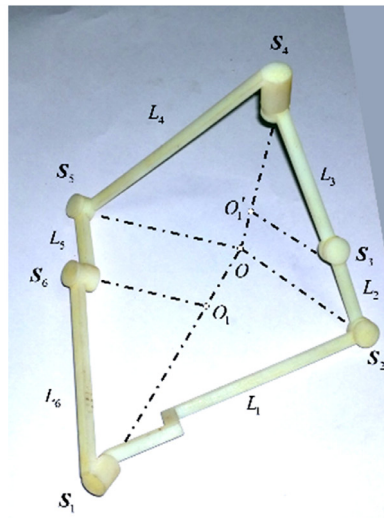
$$\begin{pmatrix}\theta_1\\\theta_2\\\theta_3\end{pmatrix} = \begin{pmatrix}\theta_4\\\theta_5\\\theta_6\end{pmatrix} \tag{12}$$

Eliminating θ_2 and θ_3, it derives

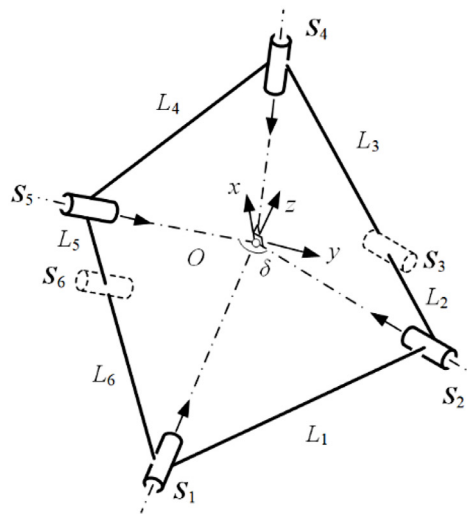$$\cos\theta_6\sin\theta_1 + \frac{\sqrt{2}}{2}\sin\theta_6\cos\theta_1 + \frac{\sqrt{2}}{2}\cos\theta_1 = -\frac{\sqrt{2}}{2} - \frac{\sqrt{2}}{2}\sin\theta_6 \tag{13}$$

Eq. (13) is then rewritten as

$$\cos\frac{\theta_1}{2}\left(\sin\frac{\theta_6}{2} + \cos\frac{\theta_6}{2}\right)\left(2\sin\frac{\theta_1}{2}\left(\cos\frac{\theta_6}{2} - \sin\frac{\theta_6}{2}\right) + \sqrt{2}\cos\frac{\theta_1}{2}\left(\sin\frac{\theta_6}{2} + \cos\frac{\theta_6}{2}\right)\right) = 0 \tag{14}$$

Fig. 4. The configuration of deployed spherical motion branch and its geometric model. (a). Deployed spherical motion branch. (b). Geometric model of deployed spherical motion branch with S3, S6 geometrically locked.

Solving Eq. (14), it yields

$$\sin \frac{\theta_6}{2} + \cos \frac{\theta_6}{2} = 0 \tag{15}$$

$$\cos \frac{\theta_1}{2} = 0 \tag{16}$$

$$2 \sin \frac{\theta_1}{2} \left(\cos \frac{\theta_6}{2} - \sin \frac{\theta_6}{2} \right) + \sqrt{2} \cos \frac{\theta_1}{2} \left(\sin \frac{\theta_6}{2} + \cos \frac{\theta_6}{2} \right) = 0 \tag{17}$$

Each of Eqs. (15)–(17) gives the geometric constrain for the joint angles of the linkage. These constraints further indicate there are three motion branches.

3. Deployed spherical motion branch and its reconfiguration

3.1. Motion analysis of deployed spherical motion branch

With the constraints in Eq. (15), it derives $\theta_6 = -\frac{\pi}{2}$, meaning joint $\mathbf{S}_6$ is geometrically locked and joint $\mathbf{S}_1$ can move independently. Hence, the linkage changes to a deployed spherical motion branch, of which the physical model and corresponding kinematic model are illustrated in Fig. 4(a) and Fig. 4(b) respectively. Substituting $\theta_6 = -\frac{\pi}{2}$ into Eq. (12), it gives $\theta_3 = -\frac{\pi}{2}$. Thus, joint $\mathbf{S}_3$ is geometrically locked and only joints 1, 2, 4 and 5 can rotate in the deployed spherical motion branch.

The direction of $\mathbf{S}_1$ is

$$\mathbf{s}_1 = (0, 0, 1)^\mathrm{T} \tag{18}$$

Thus

$$\mathbf{S}_1 = (0, 0, 1, 0, 0, 0)^\mathrm{T} \tag{19}$$

According to Dai [38–40], $\mathbf{S}_6$ is obtained using screw operator as

$$\mathbf{S}_6 = \begin{bmatrix} \mathbf{R}_{z,-\theta_1} & \mathbf{0} \\ [(-d_1\mathbf{z})\times]\mathbf{R}_{z,-\theta_1} & \mathbf{R}_{z,-\theta_1} \end{bmatrix} \begin{bmatrix} \mathbf{R}_{\mathbf{x},-\alpha_{61}} & \mathbf{0} \\ [(-a_{61}\mathbf{x})\times]\mathbf{R}_{\mathbf{x},-\alpha_{61}} & \mathbf{R}_{\mathbf{x},-\alpha_{61}} \end{bmatrix} (0, 0, 1, 0, 0, 0)^\mathrm{T} \tag{20}$$

where $(0, 0, 1, 0, 0, 0)^\mathrm{T}$ is the original screw before operation, $[(-d_1\mathbf{z})\times]$ and $[(-a_{61}\mathbf{x})\times]$ are the skew symmetry matrices of $-d_1\mathbf{z}$ and $-a_{61}\mathbf{x}$, $\mathbf{x}$ and $\mathbf{z}$ are vectors corresponding x axis and z axis, $\mathbf{R}_{z,-\theta_1}$ is the rotation matrix around z axis and the angle is $-\theta_1$, $\mathbf{R}_{\mathbf{x},-\alpha_{61}}$ is the rotation matrix around x axis and the angle is $-\alpha_{61}$. From Euler-Rodrigues formulas, we have

$$\mathbf{R}_{v,\alpha} = \mathbf{I} + \sin\alpha[v\times] + (1-\cos\alpha)[v\times]^2 \tag{21}$$

where $\mathbf{I}$ is 3×3 unit matrix, $[v\times]$ is the skew symmetry matrix of vector $\mathbf{v}$, α is the rotation angle. Substituting all the parameters of the linkage into Eq. (20), we obtain

$$\mathbf{S}_6 = \left(\frac{\sqrt{2}}{2}\sin\theta_1, \frac{\sqrt{2}}{2}\cos\theta_1, \frac{\sqrt{2}}{2}, \frac{l}{5}\cos\theta_1, -\frac{l}{5}\sin\theta_1, 0 \right)^\mathrm{T} \tag{22}$$

For deployed spherical motion branch, joint 6 is geometrically locked at $\theta_6 = -\frac{\pi}{2}$ and this gives

$$\mathbf{S}_5 = \left(\frac{\sqrt{2}}{2}\sin\theta_1, \frac{\sqrt{2}}{2}\cos\theta_1, \frac{\sqrt{2}}{2}, 0, 0, 0 \right)^\mathrm{T} \tag{23}$$

For $\mathbf{S}_2$, we have

$$\mathbf{S}_2 = \begin{bmatrix} \mathbf{R}_{\mathbf{x},\alpha_{12}} & \mathbf{0} \\ [(a_{12}\mathbf{x})\times]\mathbf{R}_{\mathbf{x},\alpha_{12}} & \mathbf{R}_{\mathbf{x},\alpha_{12}} \end{bmatrix} (0, 0, 1, 0, 0, 0)^\mathrm{T} \tag{24}$$

Substituting all the parameters of the linkage into Eq. (24), we obtain

$$\mathbf{S}_2 = \left(0, -\frac{\sqrt{2}}{2}, \frac{\sqrt{2}}{2}, 0, 0, 0 \right)^\mathrm{T} \tag{25}$$

For $\mathbf{S}_3$ and $\mathbf{S}_4$, we have

$$\mathbf{S}_3 = \left(0, -\frac{\sqrt{2}}{2}, \frac{\sqrt{2}}{2}, \frac{l}{5}\sin\theta_2, -\frac{\sqrt{2}l}{10}\cos\theta_2, -\frac{\sqrt{2}l}{10}\cos\theta_2 \right)^\mathrm{T} \tag{26}$$

$$\mathbf{S}_4 = \left(-\frac{\sqrt{2}}{2}\cos\theta_2, -\frac{1}{2}\sin\theta_2 - \frac{1}{2}, -\frac{1}{2}\sin\theta_2 + \frac{1}{2}, 0, 0, 0 \right)^\mathrm{T} \tag{27}$$

Regarding link L_4 as the moving platform and link L_1 as the base of the linkage, we have two limbs for the linkage. One limb consists of $\mathbf{S}_2$, $\mathbf{S}_3$ and $\mathbf{S}_4$, and the other limb consists of $\mathbf{S}_1$, $\mathbf{S}_6$ and $\mathbf{S}_5$. According to Dai [39,40], Dai et al. [41], the sub-chain motion-screw systems are

$$\mathbb{S}_{l1} = \{\mathbf{S}_1, \mathbf{S}_6, \mathbf{S}_5\} \tag{28}$$

$$\mathbb{S}_{l2} = \{\mathbf{S}_2, \mathbf{S}_3, \mathbf{S}_4\} \tag{29}$$

The sub-chain constraint-screw systems are

$$\mathbb{S}_{l1}^r = \begin{cases} \mathbf{S}_{11}^r = (0, 0, 1, 0, 0, 0)^T \\ \mathbf{S}_{12}^r = \left(0, 0, 0, -\frac{\sqrt{2}}{2}\cos\theta_1, \frac{\sqrt{2}}{2}\sin\theta_1, 0\right)^T \\ \mathbf{S}_{13}^r = \left(\frac{\sqrt{2}}{2}\sin\theta_1, \frac{\sqrt{2}}{2}\cos\theta_1, \frac{\sqrt{2}}{2}, 0, 0, 0\right)^T \end{cases} \tag{30}$$

and

$$\mathbb{S}_{l2}^r = \begin{cases} \mathbf{S}_{21}^r = \left(0, -\frac{\sqrt{2}}{2}, \frac{\sqrt{2}}{2}, 0, 0, 0\right)^T \\ \mathbf{S}_{22}^r = \left(0, 0, 0, \frac{\sqrt{2}}{2}\sin\theta_2, -\frac{1}{2}\cos\theta_2, -\frac{1}{2}\cos\theta_2\right)^T \\ \mathbf{S}_{23}^r = \left(-\frac{\sqrt{2}}{2}\cos\theta_2, -\frac{1}{2}\sin\theta_2 - \frac{1}{2}, -\frac{1}{2}\sin\theta_2 + \frac{1}{2}, 0, 0, 0\right)^T \end{cases} \tag{31}$$

Eqs. (30) and (31) give the common constraint-screw multiset

$$\langle\mathbb{S}^c\rangle = \langle\mathbb{S}_{l1}^r\rangle \cap \langle\mathbb{S}_{l2}^r\rangle = \emptyset \tag{32}$$

The output-link constraint-screw multiset is

$$\langle\mathbb{S}^r\rangle = \mathbb{S}_{l1}^r \uplus \mathbb{S}_{l2}^r = \langle\mathbf{S}_{11}^r, \mathbf{S}_{12}^r, \mathbf{S}_{13}^r, \mathbf{S}_{21}^r, \mathbf{S}_{22}^r, \mathbf{S}_{23}^r\rangle \tag{33}$$

Eqs. (32) and (33) give the complementary constraint-screw multiset

$$\langle\mathbb{S}_c^r\rangle = \langle\mathbb{S}^r\rangle - \langle\mathbb{S}^c\rangle = \langle\mathbf{S}_{11}^r, \mathbf{S}_{12}^r, \mathbf{S}_{13}^r, \mathbf{S}_{21}^r, \mathbf{S}_{22}^r, \mathbf{S}_{23}^r\rangle \tag{34}$$

Thus, Eq. (33) can be decomposed as

$$\langle\mathbb{S}^r\rangle = \underbrace{\emptyset}_{\langle\mathbb{S}^c\rangle} \uplus \underbrace{\{\mathbf{S}_{11}^r, \mathbf{S}_{12}^r, \mathbf{S}_{13}^r, \mathbf{S}_{21}^r, \mathbf{S}_{22}^r\}}_{\mathbb{S}_c^r} \uplus \underbrace{\{\mathbf{S}_{23}^r\}}_{\langle\mathbb{S}_v^r\rangle} \tag{35}$$

where $\langle\mathbb{S}^c\rangle$ is the common constraint-screw multiset in Eq. (32), $\mathbb{S}_c^r$ is the complementary constraint-screw system and it is the maximum linear independence group of $\langle\mathbb{S}_c^r\rangle$, $\langle\mathbb{S}_v^r\rangle$ is the redundant constraint-screw multiset and $\langle\mathbb{S}_v^r\rangle = \langle\mathbb{S}_c^r\rangle - \mathbb{S}_c^r$.

The mobility of this linkage is

$$m = b(n - g - 1) + \sum_{i=1}^{g} f_i + card\langle\mathbb{S}_c^r\rangle - dim\mathbb{S}_c^r + m_l \tag{36}$$

where b is the mobility coefficient and equals $6 - dim\mathbb{S}^c$. According to Eq. (32), $b = 6$. n is the number of the links and it is 6 for the linkage. g is the number of joints and it is 6. f_i is the mobility of joint i and it is 1 for revolute joint. $card\langle\mathbb{S}_c^r\rangle$ is the cardinal number of multiset $\langle\mathbb{S}_c^r\rangle$ and it is 6. $dim\mathbb{S}_c^r$ is the dimension of set $\mathbb{S}_c^r$ and it is 5 for the linkage. m_l is the local mobility of the linkage and it is 0 for the linkage. Substituting all the numbers into Eq. (36), we have

$$m = 1 \tag{37}$$

Further, the platform motion-screw system is

$$\mathbb{S}_f = \left\{\left(-\frac{\sqrt{2}}{2}\sin\theta_1\cos\theta_2, -\frac{\sqrt{2}}{2}\sin\theta_1\cos\theta_2, -\sin\theta_1\sin\theta_2 + \frac{\sqrt{2}}{2}\cos\theta_1\cos\theta_2, 0, 0, 0\right)^T\right\} \tag{38}$$

According to Eqs. (19), (23), (25) and (27), it proves that the linkage is a spherical 4R linkage formed by joints 1, 2, 4 and 5. Eq. (38) gives the rotation axis of link L_4.

3.2. Reconfiguration analysis of the deployed spherical motion branch

For deployed spherical motion branch, the intersection of $\mathbf{S}_1$ and $\mathbf{S}_6$ is O_1. The intersection of $\mathbf{S}_3$ and $\mathbf{S}_4$ is O_1'. When the distance between O_1 and O_1' equals zero, there is another spherical motion branch formed by joints 1, 3, 4 and 6. Because $\mathbf{S}_5$, $\mathbf{S}_6$ are parallel and $\mathbf{S}_2$, $\mathbf{S}_3$ are parallel, when $\mathbf{S}_5$ and $\mathbf{S}_2$ are collinear, there is a planar motion branch formed by joints 2, 3, 5 and 6.

The intersection O_1 is

$$O_1 = \left(0, 0, -\frac{\sqrt{2}l}{5}, 1\right)^T \tag{39}$$
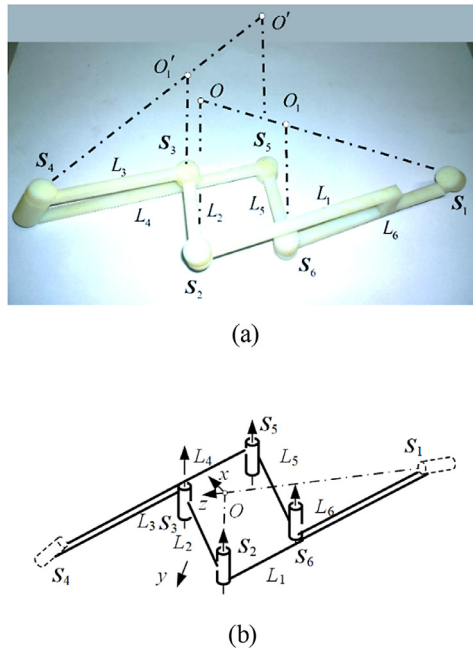
(a)

(b)

Fig. 5. The configuration of planar motion branch and its geometric model. (a). Planar motion branch. (b). Geometric model of planar motion branch with S1, S4 geometrically locked.

According to Dai [38–40], the intersection O'_1 can be obtained

$$O'_1 = \begin{bmatrix} \textbf{\textit{R}}_{\textbf{\textit{x}},\alpha_{12}} & a_{12}\textbf{\textit{x}} \\ \textbf{0}^{\mathrm{T}} & 1 \end{bmatrix} \begin{bmatrix} \textbf{\textit{R}}_{z,\theta_2} & d_2\textbf{\textit{z}} \\ \textbf{0}^{\mathrm{T}} & 1 \end{bmatrix} \begin{bmatrix} \textbf{\textit{R}}_{\textbf{\textit{x}},\alpha_{23}} & a_{23}\textbf{\textit{x}} \\ \textbf{0}^{\mathrm{T}} & 1 \end{bmatrix} \begin{bmatrix} \textbf{\textit{R}}_{z,0} & d_3\textbf{\textit{z}} \\ \textbf{0}^{\mathrm{T}} & 1 \end{bmatrix} \begin{pmatrix} 0 \\ 0 \\ 0 \\ 1 \end{pmatrix} \tag{40}$$

Substituting all the parameters of the linkage into Eq. (40), we have

$$O'_1 = \left(\frac{l}{5}\cos\theta_2, \frac{\sqrt{2}l}{10}\sin\theta_2 + \frac{\sqrt{2}l}{10}, \frac{\sqrt{2}l}{10}\sin\theta_2 - \frac{\sqrt{2}l}{10}, 1 \right)^{\mathrm{T}} \tag{41}$$

The distance between O_1 and O'_1 is

$$|O_1 O'_1| = \frac{1}{5}l\sqrt{2(1+\sin\theta_2)} \tag{42}$$

We mark δ as the angle between joint 2 and joint 5. Then

$$\delta = \arccos(\textbf{s}_{\textbf{2}} \cdot \textbf{s}_{\textbf{5}}) \tag{43}$$

where $\textbf{s}_{\mathrm{i}}$ is the direction vector of $\textbf{\textit{S}}_i$. From Eqs. (23) and (25), we have $\textbf{s}_2 = \left(0, -\frac{\sqrt{2}}{2}, \frac{\sqrt{2}}{2} \right)^{\mathrm{T}}$ and $\textbf{s}_5 = \left(\frac{\sqrt{2}}{2}\sin\theta_1, \frac{\sqrt{2}}{2}\cos\theta_1, \frac{\sqrt{2}}{2} \right)^{\mathrm{T}}$. Substituting them into Eq. (43), it gives

$$\delta = \arccos\left(\frac{1}{2}(1-\cos\theta_1) \right) \tag{44}$$

When Eq. (42) equal zero

$$\theta_2 = \frac{3}{2}\pi \tag{45}$$

When Eq. (44) equal zero

$$\theta_1 = \pi \tag{46}$$

at this configuration, $|O'_1 O''_1| = \frac{2}{5}l$.

Using the structure of the link L_4, the angle between $\textbf{\textit{S}}_4$ and $\textbf{\textit{S}}_5$ is $\frac{\pi}{4}$. This results in

$$\textbf{s}_4 \cdot \textbf{s}_5 = \frac{\sqrt{2}}{2} \tag{47}$$

From Eqs. (23) and (27), we have $\mathbf{s}_4 = \left(-\frac{\sqrt{2}}{2}\cos\theta_2, -\frac{1}{2}\sin\theta_2 - \frac{1}{2}, -\frac{1}{2}\sin\theta_2 + \frac{1}{2}\right)^{\mathrm{T}}$ and $\mathbf{s}_5 = \left(\frac{\sqrt{2}}{2}\sin\theta_1, \frac{\sqrt{2}}{2}\cos\theta_1, \frac{\sqrt{2}}{2}\right)^{\mathrm{T}}$. Substituting them into Eq. (47), we obtain one kinematic equation of deployed spherical motion branch

$$-\frac{1}{2}\sin\theta_1\cos\theta_2 - \frac{\sqrt{2}}{4}\cos\theta_1\sin\theta_2 - \frac{\sqrt{2}}{4}\cos\theta_1 - \frac{\sqrt{2}}{4}\sin\theta_2 - \frac{\sqrt{2}}{4} = 0 \tag{48}$$

It is noted that, Eqs. (45) and (46) can't make Eq. (48) right. This indicates Eqs. (45) and (46) describe two different reconfigurations for deployed spherical motion branch. When $\theta_1=\pi$, the linkage runs to the planar motion branch. When $\theta_2=\frac{3}{2}\pi$, the linkage runs to the other spherical motion branch formed by joints 1, 3, 4 and 6. The two motion branches are discussed in the next sections.

4. Planar motion branch and its reconfiguration

4.1. Motion analysis of planar motion branch

When $\theta_1=\pi$, the linkage runs to the planar motion branch in Fig. 5. For planar motion branch, Eq. (16) is right and we have

$$\theta_1=\pi \tag{49}$$

Eq. (49) indicates joint 1 is geometrically locked. According to Eq. (12), $\theta_4 = \pi$. Substituting Eq. (49) into Eqs. (9) and (10), we have

$$\cos\theta_2 + \sin(\theta_2 + \theta_3) = \cos\theta_6 \tag{50}$$

$$\sin\theta_2 - \cos(\theta_2 + \theta_3) = -1 - \sin\theta_6 \tag{51}$$

Eliminating θ_3 in Eqs. (50) and (51), we obtain

$$\sin\frac{\theta_2 + \theta_6}{2}\left(\sin\frac{\theta_2+\theta_6}{2} + \cos\frac{\theta_2 - \theta_6}{2}\right) = 0 \tag{52}$$

One solution of Eq. (52) is

$$\theta_2+\theta_6 = 2\pi \tag{53}$$

Eq. (53) results in the linkage running with both joint 2 and joint 6 rotating. This is the condition for planar motion branch.

For the limb consisting of joints 1, 6 and 5, we have

$$\mathbf{S}_1 = (0, 0, 1, 0, 0, 0)^{\mathrm{T}} \tag{54}$$

$$\mathbf{S}_6 = \left(0, -\frac{\sqrt{2}}{2}, \frac{\sqrt{2}}{2}, \frac{l}{5}, 0, 0\right)^{\mathrm{T}} \tag{55}$$

$$\mathbf{S}_5 = \left(0, -\frac{\sqrt{2}}{2}, \frac{\sqrt{2}}{2}, -\frac{l}{5} - \frac{l}{5}\sin\theta_6, -\frac{\sqrt{2}l}{10}\cos\theta_6, -\frac{\sqrt{2}l}{10}\cos\theta_6\right)^{\mathrm{T}} \tag{56}$$

For the other limb, we have

$$\mathbf{S}_2 = \left(0, -\frac{\sqrt{2}}{2}, \frac{\sqrt{2}}{2}, 0, 0, 0\right)^{\mathrm{T}} \tag{57}$$

$$\mathbf{S}_3 = \left(0, -\frac{\sqrt{2}}{2}, \frac{\sqrt{2}}{2}, \frac{l}{5}\sin\theta_2, -\frac{\sqrt{2}l}{10}\cos\theta_2, -\frac{\sqrt{2}l}{10}\cos\theta_2\right)^{\mathrm{T}} \tag{58}$$

$$\mathbf{S}_4 = \left(\mathbf{s}_4^{\mathrm{T}}, \mathbf{s}_{40}^{\mathrm{T}}\right)^{\mathrm{T}} \tag{59}$$

where

$$\mathbf{s}_4 = \left(\frac{\sqrt{2}}{2}\sin(\theta_2 + \theta_3), -\frac{1}{2}\cos(\theta_2 + \theta_3) - \frac{1}{2}, -\frac{1}{2}\cos(\theta_2 + \theta_3) + \frac{1}{2}\right)^{\mathrm{T}} \tag{60}$$

$$\boldsymbol{s}_{40} = \left(\frac{\sqrt{2}l}{10}\sin\theta_2 - \frac{\sqrt{2}l}{10}\cos(\theta_2 + \theta_3), -\frac{l}{10}\cos\theta_2 - \frac{l}{10}\sin(\theta_2 + \theta_3) + \frac{l}{10}\cos\theta_3, \right. \tag{61}$$

$$\left. -\frac{l}{10}\cos\theta_2 - \frac{l}{10}\sin(\theta_2 + \theta_3) - \frac{l}{10}\cos\theta_3 \right)^{\mathrm{T}} \tag{61}$$

Substituting Eqs. (50), (51) and (53) into Eq. (59), we have

$$\mathbf{S}_4 = \left(0, -1, 0, \frac{\sqrt{2}l}{10}\sin\theta_2 - \frac{\sqrt{2}l}{10}, 0, -\frac{l}{5}\cos\theta_2 \right)^{\mathrm{T}} \tag{62}$$

The sub-chain constraint-screw systems are

$$\mathbb{S}_{l1}^r = \begin{cases} \mathbf{S}_{11}^r = \left(0, -\frac{\sqrt{2}}{2}, \frac{\sqrt{2}}{2}, \frac{l}{5}, 0, 0 \right)^{\mathrm{T}} \\ \mathbf{S}_{12}^r = (0, 0, 0, 1, 0, 0)^{\mathrm{T}} \\ \mathbf{S}_{13}^r = \left(0, -\frac{\sqrt{2}}{2}, \frac{\sqrt{2}}{2}, 0, 0, 0 \right)^{\mathrm{T}} \end{cases} \tag{63}$$

and

$$\mathbb{S}_{l2}^r = \begin{cases} \mathbf{S}_{21}^r = \left(0, -\frac{\sqrt{2}}{2}, \frac{\sqrt{2}}{2}, \frac{l}{5}\sin\theta_2, -\frac{\sqrt{2}l}{10}\cos\theta_2, -\frac{\sqrt{2}l}{10}\cos\theta_2 \right)^{\mathrm{T}} \\ \mathbf{S}_{22}^r = (0, 0, 0, 1, 0, 0)^{\mathrm{T}} \\ \mathbf{S}_{23}^r = \left(0, -\frac{\sqrt{2}}{2}, \frac{\sqrt{2}}{2}, -\frac{l}{5} - \frac{l}{5}\sin\theta_6, -\frac{\sqrt{2}l}{10}\cos\theta_6, -\frac{\sqrt{2}l}{10}\cos\theta_6 \right)^{\mathrm{T}} \end{cases} \tag{64}$$

The output-link constraint-screw multiset is

$$\begin{aligned} \langle \mathbb{S}^r \rangle &= \mathbb{S}_{l1}^r \uplus \mathbb{S}_{l2}^r \\ &= \langle \mathbf{S}_{11}^r, \mathbf{S}_{12}^r, \mathbf{S}_{13}^r, \mathbf{S}_{21}^r, \mathbf{S}_{22}^r, \mathbf{S}_{23}^r \rangle \\ &= \underbrace{\{\mathbf{S}_{12}^r, \mathbf{S}_{22}^r\}}_{\langle \mathbb{S}^c \rangle} \uplus \underbrace{\{\mathbf{S}_{11}^r, \mathbf{S}_{13}^r, \mathbf{S}_{21}^r, \mathbf{S}_{23}^r\}}_{\mathbb{S}_c^r} \uplus \underbrace{\varnothing}_{\langle \mathbb{S}_v^r \rangle} \end{aligned} \tag{65}$$

Thus, $b = 5$, $n = 6$, $g = 6$. $card\langle \mathbb{S}_c^r \rangle = 4$ and $\dim\mathbb{S}_c^r = 4$. Substituting all the number into Eq. (36), we have $m = 1$. The platform motion-screw system is

$$\mathbb{S}_f = \left\{ \left(0, 0, 0, -\sin\theta_2, \frac{\sqrt{2}}{2}\cos\theta_2, \frac{\sqrt{2}}{2}\cos\theta_2 \right)^{\mathrm{T}} \right\} \tag{66}$$

It represents a pure translation motion along the direction $\left(-\sin\theta_2, \frac{\sqrt{2}}{2}\cos\theta_2, \frac{\sqrt{2}}{2}\cos\theta_2 \right)^{\mathrm{T}}$. According to Eqs. (55), (56), (57) and (58), the linkage is a planar 4R linkage with joints 2, 3, 5 and 6 rotating.

4.2. Reconfiguration analysis of planar motion branch

For planar motion branch, the points O and O_1 are

$$O = (0, 0, 0, 1)^{\mathrm{T}} \tag{67}$$

$$O_1 = \left(0, 0, -\frac{\sqrt{2}l}{5}, 1 \right)^{\mathrm{T}} \tag{68}$$

The intersection can be obtained using the intersection of two screws as

$$P = \left(\boldsymbol{s}_{i0} \times \boldsymbol{s}_{j0}, \boldsymbol{s}_j \cdot \boldsymbol{s}_{i0} \right)^{\mathrm{T}} \tag{69}$$

where P is the intersection of $\boldsymbol{S}_i$ and $\boldsymbol{S}_j$, $\boldsymbol{s}_i$ is the direction of $\boldsymbol{S}_i$ and $\boldsymbol{s}_{i0}$ is the secondary part of $\boldsymbol{S}_i$. Substituting Eq. (56) and Eq. (62) into Eq. (69) and making the scalar unit 1, we have

$$O' = \left(\frac{l}{5}\cos\theta_2, \frac{\sqrt{2}l}{10}\sin\theta_2 - \frac{\sqrt{2}l}{10}, \frac{\sqrt{2}l}{10}\sin\theta_2 - \frac{\sqrt{2}l}{10}, 1 \right)^{\mathrm{T}} \tag{70}$$

Substituting Eq. (58) and Eq. (62) into Eq. (69) and making the scalar unit 1, we have

$$O_1' = \left(\frac{l}{5}\cos\theta_2, \frac{\sqrt{2}l}{10}\sin\theta_2 + \frac{\sqrt{2}l}{10}, \frac{\sqrt{2}l}{10}\sin\theta_2 - \frac{\sqrt{2}l}{10}, 1 \right)^{\mathrm{T}} \tag{71}$$
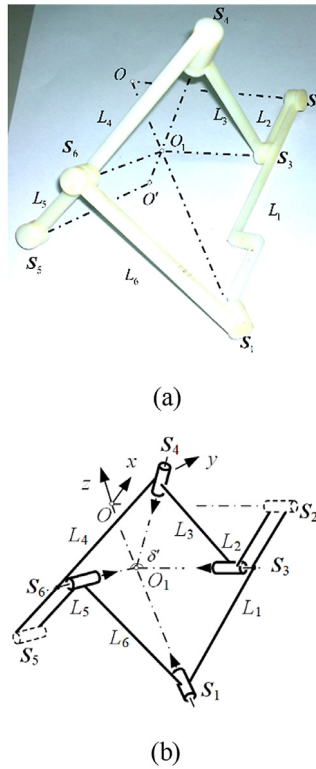
Fig. 6. One configuration of folded spherical motion branch and its geometric model. (a). Folded spherical motion branch. (b). Geometric model of folded spherical motion branch with S2, S5 geometrically locked.

Thus, the distance between O and O' is

$$|OO'| = \frac{1}{5}l\sqrt{2(1-\sin\theta_2)} \tag{72}$$

The distance between O_1 and O'_1 is

$$|O_1O'_1| = \frac{1}{5}l\sqrt{2(1+\sin\theta_2)} \tag{73}$$

According to Eqs. (72) and (73), $|OO'|$ and $|O_1O'_1|$ can't be zero at the same time. When $|OO'| = 0$, $\theta_2 = \frac{\pi}{2}$ and the linkage runs to deployed spherical motion branch. When $|O_1O'_1| = 0$, $\theta_2 = \frac{3\pi}{2}$ and the linkage runs to folded spherical motion branch discussed in the next section.

5. Analysis of folded spherical motion branch and motion branch transformation of the spherical-planar metamorphic linkage

5.1. Motion and reconfiguration analysis of folded spherical motion branch

When distance between O_1 and O'_1 becomes zero for deployed spherical motion branch and the planar motion branch, the linkage changes to folded spherical motion branch in Fig. 6 where δ' is the angle between joint 3 and joint 6.

For the folded spherical motion branch, Eq. (17) gives the kinematic equation between joint 1 and joint 6. According to Eqs. (11) and (12), $\theta_2 = \theta_5 = -\frac{\pi}{2}$, indicating joint 2 and 5 are geometrically locked.

For the limb consisting of joints 1, 6 and 5, we have

$$\mathbf{S}_1 = (0, 0, 1, 0, 0, 0)^{\mathrm{T}} \tag{74}$$

$$\mathbf{S}_5 = \left(\frac{\sqrt{2}}{2}\sin\theta_1, \frac{\sqrt{2}}{2}\cos\theta_1, \frac{\sqrt{2}}{2}, \frac{1}{5}\cos\theta_1 + \frac{1}{5}\cos\theta_1\sin\theta_6 + \frac{\sqrt{2}l}{10}\sin\theta_1\cos\theta_6, \right.$$
$$\left. -\frac{l}{5}\sin\theta_1 - \frac{l}{5}\sin\theta_1\sin\theta_6 + \frac{\sqrt{2}l}{10}\cos\theta_1\cos\theta_6, -\frac{\sqrt{2}l}{10}\cos\theta_6 \right)^{\mathrm{T}} \tag{75}$$
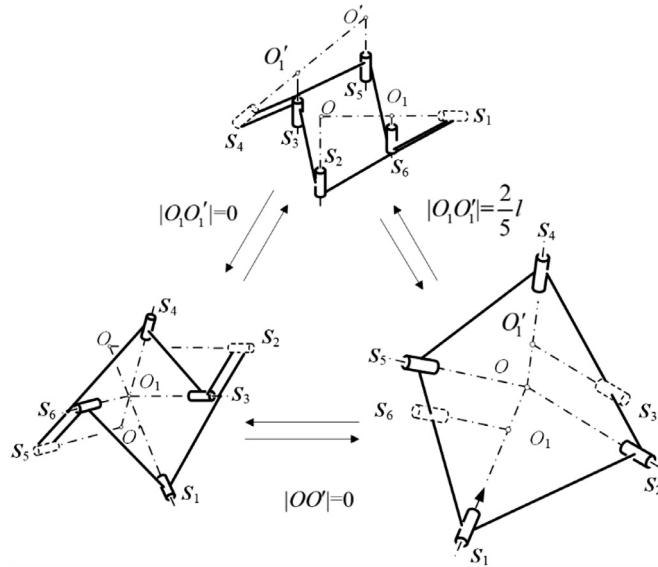
Fig. 7. Motion branch transformation of the spherical-planar metamorphic linkage.
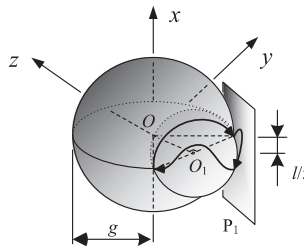

Fig. 8. Path of the point on joint 5.

$$\mathbf{S}_6 = \left(\frac{\sqrt{2}}{2}\sin\theta_1, \frac{\sqrt{2}}{2}\cos\theta_1, \frac{\sqrt{2}}{2}, \frac{1}{5}\cos\theta_1, -\frac{1}{5}\sin\theta_1, 0 \right)^{\mathrm{T}} \tag{76}$$

For the other limb, we have

$$\mathbf{S}_2 = \left(0, -\frac{\sqrt{2}}{2}, \frac{\sqrt{2}}{2}, 0, 0, 0 \right)^{\mathrm{T}} \tag{77}$$

$$\mathbf{S}_3 = \left(0, -\frac{\sqrt{2}}{2}, \frac{\sqrt{2}}{2}, -\frac{l}{5}, 0, 0 \right)^{\mathrm{T}} \tag{78}$$

$$\mathbf{S}_4 = \left(-\frac{\sqrt{2}}{2}\cos\theta_3, -\frac{1}{2}\sin\theta_3 - \frac{1}{2}, -\frac{1}{2}\sin\theta_3 + \frac{1}{2}, -\frac{\sqrt{2}l}{10} - \frac{\sqrt{2}l}{10}\sin\theta_3, \frac{1}{5}\cos\theta_3, 0 \right)^{\mathrm{T}} \tag{79}$$

Using the same method as deployed spherical motion branch and planar motion branch, the platform motion-screw system is

$$\mathbb{S}_f = \left\{ \left(\frac{1}{2}\sin\theta_1\cos\theta_3, -\frac{1}{2}\cos\theta_1\cos\theta_3, -\frac{\sqrt{2}}{2}\sin\theta_1\sin\theta_3 + \frac{1}{2}\cos\theta_1\cos\theta_3, \right. \right.$$
$$\left. \left. -\frac{\sqrt{2}l}{10}\cos\theta_1\cos\theta_3, -\frac{\sqrt{2}l}{10}\sin\theta_1\cos\theta_3, 0 \right)^{\mathrm{T}} \right\} \tag{80}$$

It is a rotation around the axis Eq. (80) decided. According to Eqs. (74), (76), (78) and (79), joints 1, 3, 4 and 6 are concurrent and the intersection is point O_1. Thus, the linkage is a spherical 4R linkage formed by joints 1, 3, 4 and 6.

According to Eq. (40), we have

$$O' = \left(-\frac{l}{5}\cos\theta_3, -\frac{\sqrt{2}l}{10} - \frac{\sqrt{2}l}{10}\sin\theta_3, -\frac{\sqrt{2}l}{10} - \frac{\sqrt{2}l}{10}\sin\theta_3, 1\right)^T \tag{81}$$

Further

$$|OO'| = \frac{1}{5}l\sqrt{2(1+\sin\theta_3)} \tag{82}$$

The angle between S_3 and S_6 is

$$\delta' = \arccos(\mathbf{s}_3 \cdot \mathbf{s}_6) \tag{83}$$

From Eqs. (76) and (78), we have $\mathbf{S}_3 = \left(0, -\frac{\sqrt{2}}{2}, \frac{\sqrt{2}}{2}\right)^T$ and $\mathbf{S}_6 = \left(\frac{\sqrt{2}}{2}\sin\theta_1, \frac{\sqrt{2}}{2}\cos\theta_1, \frac{\sqrt{2}}{2}\right)^T$. Substituting them into Eq. (83), we obtain

$$\delta' = \arccos\left(\frac{1}{2} - \frac{1}{2}\cos\theta_1\right) \tag{84}$$

Making $|OO'| = 0$, we have $\theta_3 = \frac{3\pi}{2}$. At that point the linkage runs to deployed spherical motion branch. When Eq. (84) equals zero, we obtain $\theta_1 = \frac{3\pi}{2}$ and the linkage runs to planar motion branch .

5.2. Motion branch transformation and their close loop

All three motion branches are deployed spherical motion branch, planar motion branch and folded spherical motion branch. It is noted that the linkage runs from deployed spherical motion branch to planar motion branch. Then from planar motion branch, it runs to folded spherical motion branch and back to the original configuration. Also, it can change from deployed spherical motion branch to folded spherical motion branch directly. The process is shown in Fig. 7.

It is noted that during the transformation, $|OO'|$ and $|O_1O'_1|$ describe the condition for the deployed spherical motion branch and folded spherical motion branch. δ and δ' describe the conditions for planar motion branch. They can be used as transition indexes to describe the transition. We will use the transition index in the next section and give a Bennett-spherical 6R metamorphic linkage.

Because the motion of the three motion branches, points on L_4 can transform from a sphere to a plane. The path of a point on S_5 is

$$\mathbf{r} = \begin{cases} \left(-\frac{\sqrt{2}}{2}g\sin\theta_1, -\frac{\sqrt{2}}{2}g\cos\theta_1, -\frac{\sqrt{2}}{2}g\right)^T \text{deployed spherical motion} \\ \left(\frac{l}{5}\cos\theta_2, \frac{\sqrt{2}l}{10}\sin\theta_2 - \frac{\sqrt{2}l}{10} + \frac{\sqrt{2}}{2}g, \frac{\sqrt{2}l}{10}\sin\theta_2 - \frac{\sqrt{2}l}{10} - \frac{\sqrt{2}}{2}g\right)^T \text{planar motion} \\ \left(-\frac{l}{5}\cos\theta_3 - \frac{\sqrt{2}}{2}g\sin\theta_1, -\frac{\sqrt{2}l}{10} - \frac{\sqrt{2}l}{10}\sin\theta_3 - \frac{\sqrt{2}}{2}g\cos\theta_1, \right. \\ \left. -\frac{\sqrt{2}l}{10} - \frac{\sqrt{2}l}{10}\sin\theta_3 - \frac{\sqrt{2}}{2}g\right)^T \quad \text{folded spherical motion} \end{cases} \tag{85}$$

where g is the distance from O to the point. When we choose one path from deployed spherical motion branch with $\theta_1 \in [0, \pi]$, one path from planar motion branch with $\theta_2 \in [\frac{\pi}{2}, \frac{3\pi}{2}]$ and one path from folded spherical motion branch with $\theta_3 \in [\frac{\pi}{2}, -\frac{\pi}{2}]$, we obtained a close loop path. According to Eqs. (9), (10), (11) and (85), the close loop path is shown in Fig. 8. There are a large sphere, a plane and a smaller sphere in Fig. 8. O is the center of the large sphere and we mark it as sphere O. O_1 is the center of the smaller sphere and we mark it as sphere O_1. The plane is marked as P_1. The close loop path consists of three parts. One part is on the sphere O and one part is on plane P_1. The last part is on the sphere O_1. Thus, the point can move from the lager sphere O to a plane and then back to the original point the by a different path on the smaller sphere O_1. O and O_1 are two motion centers of the linkage and the path can transform between the two paths on the two spheres.

6. Bennett-spherical 6R metamorphic linkage from deployed Bennett motion branch to spherical motion branch

6.1. Bennett-spherical 6R metamorphic linkage

Using the transition index and making it zero, we design a new linkage from the Bennett linkage. Fig. 9(a). shows the original Bennett linkage. The parameters of the original linkage are
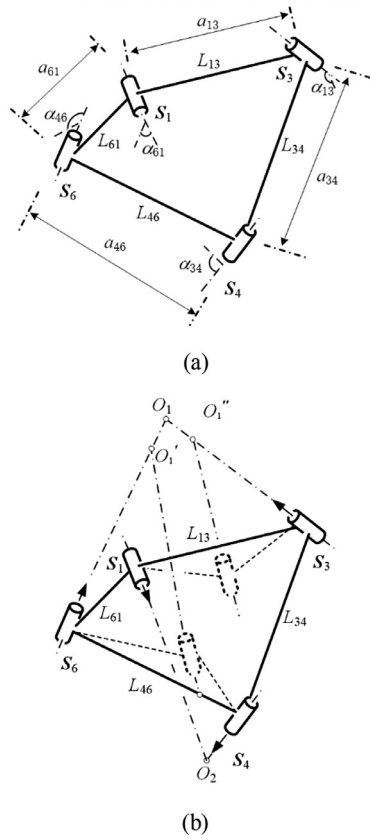
Fig. 9. Original Bennett linkage and its converting to the metamorphic linkage. (a). Parameters of the original Bennett linkage. (b). Converting the Bennett linkage to the Bennett-spherical 6R metamorphic linkage.

$$a_{13} = a_{34} = a_{46} = a_{61} = 2l$$
$$\alpha_{13} = \alpha_{46} = -\frac{3\pi}{4}, \alpha_{34} = \alpha_{61} = \frac{3\pi}{4}$$
$$d_1 = d_3 = d_4 = d_6 = 0 \tag{86}$$

they satisfy the condition

$$a_{13} = a_{46} = a, a_{34} = a_{61} = b$$
$$\alpha_{13} = -\alpha_{61} = \alpha, \alpha_{34} = -\alpha_{46} = \beta \tag{87}$$
$$\frac{\sin\alpha}{a} = \frac{\sin\beta}{b}$$

Eq. (87) is the condition for Bennett linkage. Fig. 9(b) is the geometric relationship of the joints by adding two screws, where distance between O'_1 and O''_1 can be used to check reconfigurability. O_1 is the intersection of joints 1 and joint 4. O_2 is the intersection of joint 3 and joint 6. We add two joints S_2 and S_5 to the original linkage. S_2 is concurrent with S_3 at point O''_1 and S_5 is concurrent with S_6 at point O'_1. Link L_{13} is replaced by L_{12} and L_{23}. Link L_{46} is replaced by L_{45} and L_{56}. The new linkage is shown in Fig. 10(a). The D-H parameters of this new metamorphic linkage are

$$a_{12} = a_{45} = l, a_{23} = a_{56} = 0, a_{34} = a_{61} = 2l$$
$$\alpha_{12} = \alpha_{45} = -\arccos\left(-\frac{\sqrt{6}}{4}\right), \alpha_{23} = \alpha_{56} = \frac{\pi}{6}, \alpha_{34} = \alpha_{61} = \frac{3\pi}{4} \tag{88}$$
$$d_1 = d_4 = \frac{\sqrt{6}l}{5}, d_2 = d_5 = \frac{14l}{5}, d_3 = d_6 = -\sqrt{3}l$$

where the parameters a_{34}, a_{61}, a_{34} and a_{61} are the same with the parameters in Fig. 9(a), the others are in Fig. 10(b). From the D-H parameters in Eq. (88), the linkage is a special case of Bricard line-symmetric 6R linkage.

During the deployed Bennett motion branch, the distance $|O'_1 O''_1|$ changes. When it equals zero, the linkage runs to spherical motion branch.

(a)

(b)

(c)
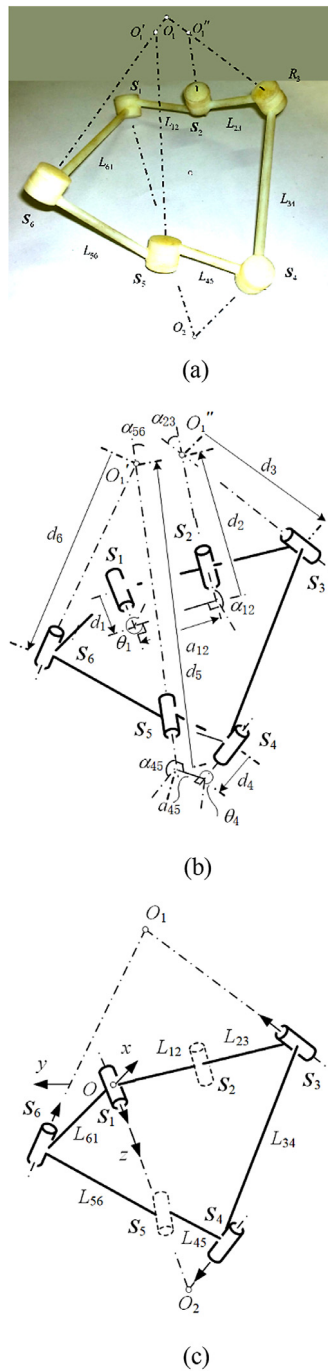
Fig. 10. The new 6R metamorphic linkage, its parameters and the geometric relationship of joints. (a). The new 6R metamorphic linkage. (b). Parameters of the new linkage. (c). Geometric model of the new metamorphic linkage and its Bennett motion branch with S2, S5 geometrically constrained.

6.2. Reconfiguration analysis from the deployed Bennett motion branch to the spherical motion branch

For the new metamorphic linkage, the coordinate frame is set on link L_{61} in Fig. 10(c). The axis of joint 1 is z axis and the direction of the common perpendicular line from joint 6 to joint 1 is x axis. y axis is decided by right-hand rule. Origin O is the intersection of joint 1 and the common perpendicular line from joint 6 to joint 1.
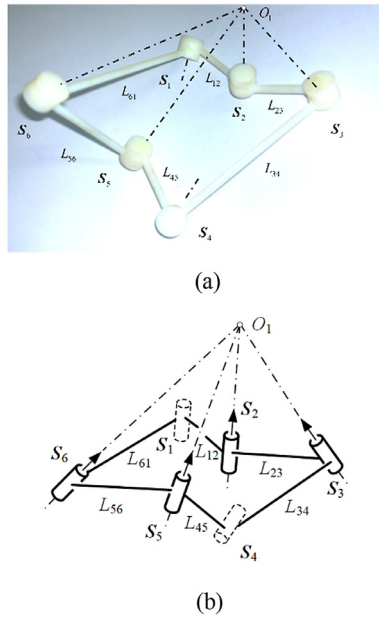
Fig. 11. One configuration of spherical motion branch and its geometric model. (a). Spherical motion branch. (b). Geometric model of special motion branch with S1, S4 being geometrically constrained to form a four-bar spherical linkage branch.

The coordinate of O'_1 is

$$O'_1 = \begin{bmatrix} \mathbf{R}_{\mathbf{x},-\alpha_{61}} & -a_{61}\mathbf{x} \\ \mathbf{0}^{\mathrm{T}} & 1 \end{bmatrix} \begin{bmatrix} \mathbf{I} & -d_6\mathbf{z} \\ \mathbf{0}^{\mathrm{T}} & 1 \end{bmatrix} \begin{pmatrix} 0 \\ 0 \\ 0 \\ 1 \end{pmatrix} \tag{89}$$

Substituting the parameters of the linkage into Eq. (89), we have

$$O'_1 = (-2l, \frac{\sqrt{6}l}{2}, -\frac{\sqrt{6}l}{2}, 1)^{\mathrm{T}} \tag{90}$$

For O''_1, we have

$$O''_1 = \begin{bmatrix} \mathbf{R}_{\mathbf{z},\theta_1} & d_1\mathbf{z} \\ \mathbf{0}^{\mathrm{T}} & 1 \end{bmatrix} \begin{bmatrix} \mathbf{R}_{\mathbf{x},\alpha_{12}} & a_{12}\mathbf{x} \\ \mathbf{0}^{\mathrm{T}} & 1 \end{bmatrix} \begin{bmatrix} \mathbf{I} & d_2\mathbf{z} \\ \mathbf{0}^{\mathrm{T}} & 1 \end{bmatrix} \begin{pmatrix} 0 \\ 0 \\ 0 \\ 1 \end{pmatrix} \tag{91}$$

Thus

$$O''_1 = \left(\left(\cos\theta_1 - \frac{7\sqrt{10}}{10}\sin\theta_1 \right)l, \left(\sin\theta_1 + \frac{7\sqrt{10}}{10}\cos\theta_1 \right)l, -\frac{\sqrt{6}l}{2}, \mathbf{1} \right)^{\mathrm{T}} \tag{92}$$

where θ_1 is the joint angle as shown in Fig. 10(b).

The distance is

$$|O'_1 O''_1| = l\sqrt{\left(\cos\theta_1 - \frac{7\sqrt{10}}{10}\sin\theta_1 + 2 \right)^2 + \left(\sin\theta_1 + \frac{7\sqrt{10}}{10}\cos\theta_1 - \frac{\sqrt{6}}{2} \right)^2} \tag{93}$$

When Eq. (93) equals zero, $\theta_1 = \arccos(\frac{7\sqrt{15}-20}{59})$. According to Baker [35], $\theta_4 = \theta_1 = \arccos(\frac{7\sqrt{15}-20}{59})$. θ_4 is the joint angle as shown in Fig. 10(b). This is the condition for the linkage running to spherical motion branch in Fig. 11.

6.3. The third motion branch and the motion branch transformation to the folded Bennett motion branch
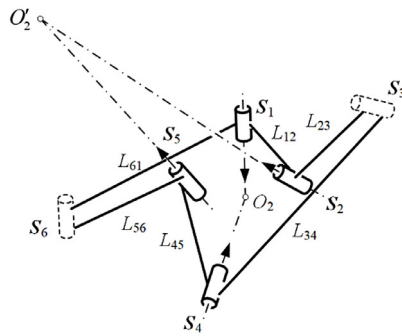
Except the original deployed Bennett motion branch and the spherical motion branch, there is another motion branch formed by joints 1, 2, 4 and 5. When the deployed Bennett motion branch comes to the configuration to make joint 3
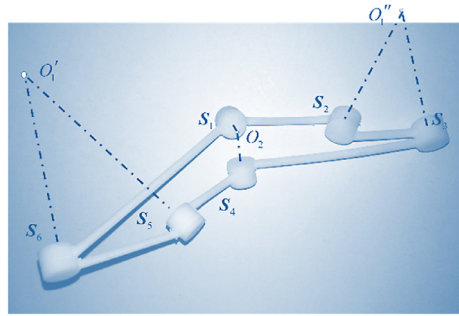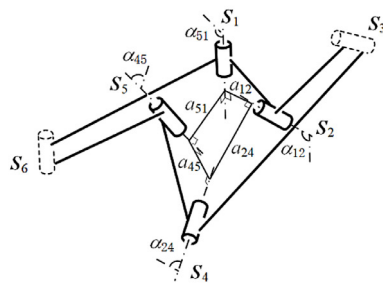
(a)
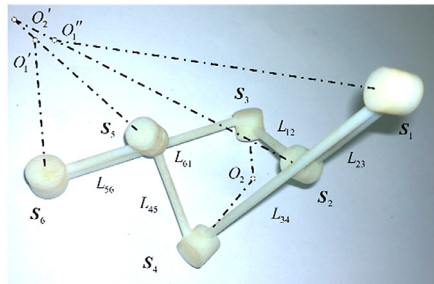
(b)

(c)

(d)

Fig. 12. The configuration of folded Bennett motion branch formed by joints 1, 2, 4, 5 and its geometric model. (a). The transformation configuration between deployed Bennett motion branch and folded Bennett motion branch. (b). Folded Bennett motion branch formed by joints 1, 2, 4, 5. (c). Geometric model of the folded Bennett motion branch formed by joints 1, 2, 4, 5 with S3, S6 geometrically constrained.
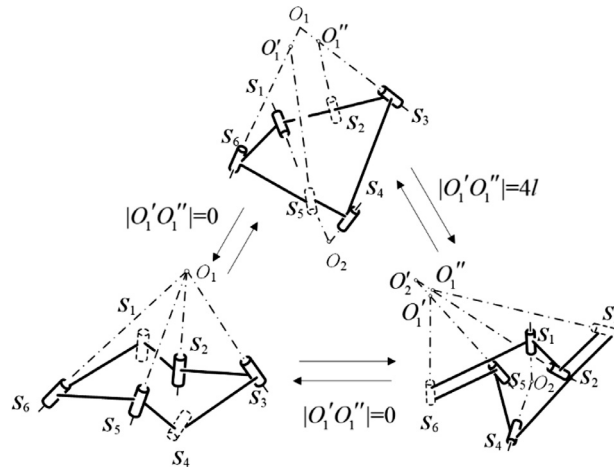
Fig. 13. Motion branch transformation of the Bennett-spherical 6R metamorphic linkage.

parallel with joint 6 in Fig. 12(a), it will turn to the folded Bennett motion branched in Fig. 12(b). For this motion branch, we have

$$a_{12} = a_{45} = l = a', a_{24} = a_{51} = l = b'$$
$$\alpha_{12} = -\alpha_{45} = -\arccos(-\tfrac{\sqrt{6}}{4}) = \alpha', \alpha_{24} = -\alpha_{51} = -\arccos(-\tfrac{\sqrt{6}}{4}) = \beta' \tag{94}$$
$$\frac{\sin\alpha'}{a'} = \frac{\sin\beta'}{b'}$$

where all the parameters are in Fig. 12(d).

Thus, this motion branch is folded Bennett motion branch, but it is different from the motion branch in Fig. 9(a). For this motion branch, when Eq. (93) equals zero, the linkage runs to the spherical motion branch. When $|O_1'O_1''| = 4l$ making joint 3 parallel with joint 6, Bennett motion branch formed by joints 1, 3, 4, 6 transforms to folded Bennett motion branch formed by joints 1, 2, 4, 5.

The transformation is shown in Fig. 13. The three motion branches form a close loop. The linkage can run from the deployed Bennett motion branch in Fig. 9 to the spherical motion branch in Fig. 11, then to the folded Bennett motion branch in Fig. 12. Also, it can transform directly from the deployed Bennett motion branch in Fig. 9 to the folded Bennett motion branch in Fig. 12.

7. Conclusions

This paper presented two novel 6R metamorphic linkages as the spherical-planar metamorphic linkage and the Bennett-spherical metamorphic linkage with each of them having three motion branches. The Spherical-planar 6R metamorphic linkage was originated from a kirigami and has two deployed and folded spherical motion branches and one planar motion branch. When the distance between two intersections of joint axes becomes zero, the linkage turns to a spherical motion branch. When the angle between two groups of parallel joints becomes zero , the linkage turns to the planar motion branch. The Bennett-spherical 6R metamorphic linkage is obtained by making the distance between two intersections of joint axes zero, the linkage then has two deployed and folded Bennett motion branches and one spherical motion branch. The reconfiguration analysis of both linkages was carried out and the geometrical constraints for motion branch transformations are revealed.

The paper further developed the close-loop equations, gave the kinematic equations for different motion branches and used screw theory to analyze motion of each motion branch. It is found that when the close-loop equation has different solutions, the linkage gives different motion branches. Using calculation, the transition index was obtained and used to analyze the reconfiguration of the linkages.

Between the deployed spherical and folded spherical motion branches in the spherical-planar 6R metamorphic linkage and between the deployed Bennett and folded Bennett motion branches in the Bennett-spherical 6R metamorphic linkage, it was found that the deployable motion branch has higher reconfigurability.

References

[1] K. Kutzbach, Mechanische, leitungsverzweigung, ihre gesetze und anwendungen, Maschinenbau 8 (21) (1929) 710–716.
[2] P.T. Sarrus, Note sur la transformation des mouvements rectilignes alternatifs, en mouvements circulaires, et reciproquement, Académie des Sciences 36 (1853) 1036–1038.
[3] R. Bricard, Mémoire sur la théorie de l'octaedre articulé, Journal de Mathématiques Pures et Appliquées, Liouville 3 (1897) 113–148.
[4] R. Bricard, Leçons de cinématique, Tome II Cinématique Appliquée, Gauthier-Villars, Paris, 1927, pp. 7–12.
[5] F.E. Myard, Contribution à la géométrie des systèmes articulés, Bulletin de la Société Mathématique de France 59 (1931) 183–210.
[6] G.T. Bennett, A new mechanism, Engineering 76 (1903) 777–778.
[7] P. Schatz, Mechanism producing wavering and rotating movements of receptacles, 1942, US, US2302804.
[8] M. Goldberg, New five-bar and six-bar linkages in three dimensions, Trans. ASME 65 (1943) 649–663.
[9] P.G. Altmann, Communications to Grodzinski, P. and M'Ewen, E., Link mechanisms in modern kinematics, in: Proceedings of the Institution of Mechanical Engineers, 168, 1954, pp. 877–896.
[10] K.J. Waldron, Hybrid over-constrained linkages, J. Mech. 3 (2) (1968) 73–78.
[11] J.E. Baker, An analysis of the Bricard linkages, Mech. Mach. Theory 15 (4) (1980) 267–286.
[12] K. Wohlhart, Merging two general Goldberg 5R linkages to obtain a new 6R space mechanism, Mech. Mach. Theory 26 (2) (1991) 659–668.
[13] Y. Chen, Z. You, Spatial 6R linkages based on the combination of two Goldberg 5R linkages, Mech. Mach. Theory 42 (2007) 1484–1498.
[14] L. Cui, J.S. Dai, Axis constraint analysis and its resultant 6R double-centered over-constrained mechanisms, Trans. ASME: J. Mech. Robot. 3 (3) (2011) 031004.
[15] K. Zhang, J.S. Dai, in: Kinematics of an Over-Constrained 6R Linkage With 2-fold Rotational symmetry, Latest Advances in Robot Kinematics, Springer, Netherlands, 2012, pp. 229–236.
[16] X. Kong, Type synthesis of single-loop over-constrained 6R spatial mechanisms for circular translation, Trans. ASME: J. Mech. Robot. 6 (16) (2014) 041016.
[17] K. Wohlhart, in: Kinematotropic linkages, Recent Advances in Robot Kinematics, Springer, Dordrech, 1996, pp. 359–368.
[18] J.S. Dai, J.R. Jones, Mobility in metamorphic mechanisms of foldable/erectable kinds, Trans. ASME: J. Mech. Des. 121 (3) (1999) 375–382.
[19] J.S. Dai, J.R. Jones, Matrix representation of topological changes in metamorphic mechanisms, Trans. ASME: J. Mech. Des. 127 (4) (2005) 837–840.
[20] C. Galletti, P Fanghella, Single-loop kinematotropic mechanisms, Mech. Mach. Theory 36 (6) (2001) 743–761.
[21] H.Y. Yan, N.T. Liu, Finite-state-machine representations for mechanisms and chains with variable topologies, in: Proceedings of ASME Design Engineering Technical Conference, Baltimore, Maraland, 2000, pp. 10–13.
[22] C.C. Lee, J.M. Hervé, Discontinuous mobility of four-link mechanisms with revolute, prismatic and cylindric pairs through the group algebraic structure of the displacement set, in: Proc. VIII International Conference on the Theory of Machines and Mechanisms, Liberec, Czech Republic, 2000, pp. 377–382.
[23] D. Gan, J.S. Dai, Q. Liao, Mobility change in two types of metamorphic parallel mechanisms, Trans. ASME J. Mech. Robot. 1 (4) (2009) 041007.
[24] K. Zhang, J.S. Dai, Y. Fang, Geometric constraint and mobility variation of two 3SvPSv metamorphic parallel mechanisms, Trans. ASME J. Mech. Des, 135 (1) (2013) 011001.
[25] C.Y. Song, Y. Chen, I.M. Chen, A 6R linkage reconfigurable between the line-symmetric Bricard linkage and the Bennett linkage, Mech. Mach. Theory 70 (2011) 278–292.
[26] K. Zhang, J.S. Dai, A kirigami-inspired 8R linkage and its evolved over-constrained 6R linkages with the rotational symmetry of order two, Trans. ASME: J. Mech. Robot. 6 (2) (2014) 021007.
[27] W. Ye, Y. Fang, K. Zhang, S. Guo, A new family of reconfigurable parallel mechanisms with diamond kinematotropic chain, Mech. Mach. Theory 74 (2014) 1–9.
[28] K. Zhang, J.S. Dai, Trifurcation of the evolved sarrus-motion linkage based on parametric constraints, in: Advances in Robot Kinematics, Springer International Publishing, 2014, pp. 345–353.
[29] Y. Qin, J.S. Dai, G. Gogu, Multi-furcation in a derivative queer-square mechanism, Mech. Mach. Theory 81 (2014) 36–53.
[30] L. Zhang, J.S. Dai, Reconfiguration of spatial metamorphic mechanisms, Trans. ASME: J. Mech. Robot. 1 (1) (2009) 011012.
[31] S. Li, J.S. Dai, Augmented adjacency matrix for topological configuration of the metamorphic mechanisms, J. Adv. Mech. Des. Syst. Manuf. 5 (5) (2011) 187–198.
[32] K.H. Hunt, Special configurations of robot-arms via screw theory, Robotica 4 (3) (1986) 171–179.
[33] K. Sugimoto, J. Duffy, K.H. Hunt, Special configurations of spatial mechanisms and robot arm, Mech. Mach. Theory 17 (2) (1982) 119–132.
[34] D.S. Zlatanov, I.A. Bonev, C. Gosselin, Constraint singularities as configuration space singularities, in: Advances in Robot Kinematics, Theory and Applications, Kluwer Academic Press, 2002, pp. 183–192.
[35] A. Müller, Higher derivatives of the kinematic mapping and some applications, Mech. Mach. Theory 76 (2014) 70–85.
[36] R.S. Ball, A Treatise on the Theory of Screws, Cambridge University, Cambridge, 1900.
[37] J.E. Baker, An analysis of the Bricard linkages, Mech. Mach. Theory 15 (4) (1980) 267–286.
[38] J.S. Dai, Finite displacement screw operators with embedded chasles' motion, Trans. ASME J. Mech. Robot. 4 (4) (2012) 041002.
[39] J.S. Dai, Geometrical foundations and screw algebra for mechanisms and robotics, Higher Education Press, Translation from "Dai, J.S. 2019, Screw Algebra and Kinematic Approaches For Mechanisms and Robotics, Higher Education Press, Springer, London", Beijing, China, ISBN: 9787040334838.
[40] J.S. Dai, Screw Algebra and Lie Groups and Lie Algebras, Higher Education Press, Beijing, 2014 ISBN: 9787040318456.
[41] J.S. Dai, Z. Huang, H. Lipkin, Mobility of over-constrained parallel mechanisms, Trans. ASME: J. Mech. Des. 128 (1) (2006) 220–229.